

● *Original Contribution*

## TREATMENT PLANNING FOR HEAVY ION RADIOTHERAPY†

GEORGE T.Y. CHEN, Ph.D., RAJINDER P. SINGH, Ph.D.,  
JOSEPH R. CASTRO, M.D., JOHN T. LYMAN, Ph.D.  
and JEANNE M. QUIVEY, M.D.

Radiotherapy Section, Bldg 55, Rm 121, Lawrence Berkeley Laboratory, Berkeley, CA 94720, U.S.A.

A computerized treatment planning system based on quantitative information in computerized tomographic (CT) scans has been developed for the heavy ion radiotherapy trials at the Lawrence Berkeley Laboratory. The CT number of each pixel is converted to a water equivalent length and used in the calculation of isoeffect dose distributions from multiport heavy charged particle irradiation. The water equivalent length of pixels in the beam path has also been histogrammed and used in quantitatively studying the range shortening effects by inhomogeneities. Treatment plans for representative lesions of the pelvis, abdomen, and thorax are presented.

Heavy ion radiotherapy, Computerized tomography treatment planning.

### INTRODUCTION

The use of heavy charged particles in radiotherapy may provide a therapeutic gain as a result of an improved dose distribution and the potential of a biologic advantage.<sup>3</sup> In order to test the value of this new modality, the technical problems of dose delivery must be adequately understood and solved. One such aspect is the development of computerized treatment planning, which will reflect realistically the isoeffect distributions from multiport heavy ion therapy in the presence of inhomogeneities. In this article, we describe the development of a computerized tomography (CT) based treatment planning program and present typical treatment plans for several sites of interest to the heavy ion radiotherapy trials under way at the Lawrence Berkeley Laboratory.<sup>4</sup>

### METHODS AND MATERIALS

#### *Beam properties*

*Finite range.* The finite range of charged particles is the principal source of an improved physical dose distribution over photon therapy. Beam depth of penetration is determined by the initial energy of the

particles and the properties of the medium traversed. Accelerated beams of helium, carbon, neon, and argon ions are available with sufficient energy to pass through beam scattering foils and ridge filters and still have a penetration range in the patient of at least 25 cm of water. From our experience with helium ions, a maximum residual range of about 26 cm is adequate for most deep seated lesions in the abdomen and pelvis, including the range shortening effects of bone. A frequency analysis of residual ranges used in 33 patients showed an average range of  $20.5 \pm 3.9$  cm of water. The physical dose rates for these beams as measured at the proximal peak, range from 250 rad/min/liter for carbon to 35 rad/min/liter for argon. Folding in the high relative biological effectiveness (RBE) for these heavy ions increases the effectiveness of these beams relative to conventional radiations by a factor of from 2 to 3.<sup>2</sup> This results in treatment times of typically 1-2 min.

By appropriate use of a variable water column and 3 dimensional compensation, the depth of penetration may be adjusted precisely to cover the tumor volume adequately and minimize the dose to critical tissues distal to the target. However, in order to exploit this

†Presented at the 19th Annual Meeting, American Society of Therapeutic Radiologists, Denver, Colorado, U.S.A. (1977).

Supported by National Institutes of Health-National Cancer Institute (NIH-NCI) Grants No. 5PO1CA19138 and 2PO1CA19138 and by Energy Research Development Agency (ERDA) Contract W-7405 Eng 48.

*Acknowledgements*—The authors wish to thank Dr. Douglas Boyd of the University of California, San Francisco for the use of his CT phantom and for many valuable comments, and Dr. Samuel Pitluck for his assistance in computer programming.

Accepted for publication 28 March 1979.

potential advantage properly, the appropriate water equivalent depth of penetration must be determined accurately. This parameter is the single most important quantity to be defined in order to position the beam precisely in depth. Because of the sharp dose gradient at the distal end of the beam, an incorrect calculation of the depth of penetration could lead to a significant underdose of the target or an undesirable overdose of sensitive tissues distal to the tumor. The quantitative information necessary to characterize the inhomogeneities in the beam path and to determine the appropriate treatment depth is obtained from CT data. Details of the method used are presented later.

#### Ridge filtered beams

The narrow Bragg peaks of heavy ions are broadened to therapeutically useful dimensions by spiral ridge filters.<sup>11</sup> Since the RBE increases toward the end of the range, the physical dose is decreased near the distal end of the ridge filtered beam in order to produce a region of uniform biological effect. The biophysical model used to calculate the physical dose distribution required for isosurvival over a desired depth is described elsewhere.<sup>4</sup> The physical dose dis-

tribution of a family of ridge filtered carbon beams is shown in Fig. 1a. This series of ridge filtered beams is designed to produce regions of uniform biological effect from 2 to 14 cm in depth in 2 cm increments. The curves are arbitrarily normalized at the distal edge. The corresponding Cobalt-Rad-Equivalent (CoRE) dose distributions is shown in Fig. 1b. A CoRE distribution is the low LET depth dose profile equivalent to the biological effect produced by the heavy charged particle beam. These curves are also called isoeffect depth dose distributions because they produce uniform biological effect over their flat top regions. The physical dose distributions of the carbon beams in Fig. 1a are designed to produce the isoeffect distributions in Fig. 1b. Isoeffect distributions for helium and neon are shown in Figs. 1c and 1d. These isoeffect depth dose distributions are the principal source of beam data used in treatment planning calculations.

The carbon and neon beams exhibit tails in the dose distributions which result from the production of nuclear fragments as the primary beam traverses the medium. These lighter fragments have a slightly longer range than the parent nuclei and result in dose past the stopping point of the primary beam. For carbon, the tail dose is initially 30% and falls to 15% within 10 additional centimeters of water. The specific amount of fragmentation is dependent on the initial energy of the beam. A lower energy beam will result in a lower fragmentation dose, but would have a shorter residual range.

The entrance dose of heavy ion beams is dependent upon the ridge filter specification and ion type. The helium skin dose from a single port ranges from 60% for a 6 cm ridge filter, to 80% for a 14 cm ridge filter, while for neon, the corresponding values are 75 and 92% respectively. The use of opposing or multiple ports with particle beams reduces the skin dose to well-tolerated levels.

#### Sharp penumbras

Heavy ion beams exhibit sharp lateral penumbras. In the plateau region of the depth dose curve, the lateral dose has been measured to fall from 90 to 10% in 3.5 mm for the helium beam. As the beam energy decreases, multiple Coulomb scattering increases, and the penumbra in the isosurvival region of the ridge filtered helium beam increases to 10 mm. The carbon and neon penumbras are a factor of about 2 smaller than the helium values because of the increased particle mass. In treatment planning calculations, the helium penumbra is modelled by a Gaussian fall off with parameters obtained from experimental measurements. For carbon and neon, the penumbras are extremely sharp, and are smaller than the grid spacing of the calculation matrix. In these cases, the

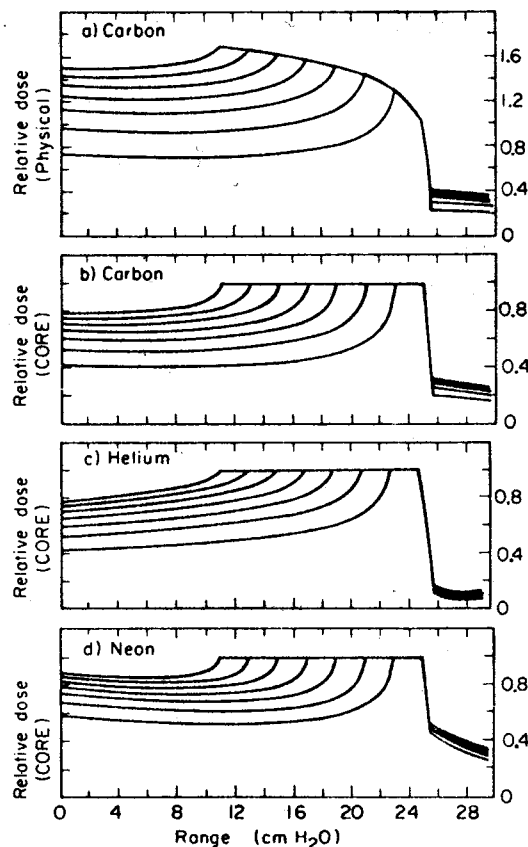


Fig. 1. (a) Physical depth dose distribution of a family of carbon ridge filtered beams. (b) Corresponding isoeffect distributions for carbon beams. (c) Isoeffect distributions for helium beams (d) Isoeffect distributions for neon beams.

penumbra dose is calculated to fall from the 100% level to the 0% level within one lateral pixel.

#### Use of CT data

CT data are used to define the position of the treatment volume relative to critical structures and to quantify the inhomogeneities which perturb the particle beams.

The CT value of each pixel must be converted to a water equivalent path length in order to provide the expected change in residual range of the beam. CT numbers are a measure of the linear attenuation coefficient of each pixel at diagnostic photon energies. At these energies, the linear attenuation coefficient is dependent upon the effective atomic number, which contributes to the photoelectric effect, and the electron density. The equation relating these quantities is shown below:<sup>14</sup>

$$\mu = \rho N_o \frac{Z}{A} [\sigma^{KN}(E) + \sigma^{PE}(E,Z)] \quad (1)$$

where

- $\rho$  = density
- $N_o$  = Avogadro's number
- $Z$  = atomic number
- $A$  = atomic weight
- $\sigma^{KN}$  = Klein Nishina cross section per electron
- $\sigma^{PE}$  = photoelectric cross section per electron

The quantity  $\rho N_o Z/A$  is the electron density of the material in electrons per cm<sup>3</sup>. The photoelectric cross section contributes to the observed CT number with a  $Z^3$  dependence. At 70 KeV (equivalent to 140 KVP), the photoelectric effect constitutes 5% of the interactions in muscle and 26% of the interactions in compact bone.<sup>9</sup>

In contrast, the equation governing energy loss of heavy charged particles in a medium (1) is:

$$\frac{dE}{dX} = \frac{k_1 \rho N_o Z}{\beta^2 A} \left[ \ln \frac{k_2 \beta^2}{I^2 (1 - \beta^2)} - 2\beta^2 \right] \quad (2)$$

where

- $k_1$  = constant including particle charge
- $\beta$  = relativistic velocity  $v/c$
- $k_2$  = constant
- $I$  = adjusted ionization potential of the medium

This equation defines a direct relation between energy loss and the electron density of the medium, with a logarithmic dependence on the adjusted ionization

potential. The ionization potential of human tissues produces a small variation in the logarithmic term. The dominant factor in determining the range shortening of charged particles is the electron density.

Since human tissues are characterized by a number of different atomic numbers and densities, the problem is to extract the water equivalent length per pixel from CT data. The required electron density may be extracted from a dual energy scan as suggested by others.<sup>12</sup> However, a precise knowledge of the effective energy and pixel registration between the dual scans complicate the use of this technique.

If approximations are made, it is possible to correlate the water equivalent length of each pixel with the CT number from a single energy scan with sufficient accuracy for clinical use. Specifically, the method used involves defining a calibration curve relating the CT numbers of tissue analogues with the observed water equivalent length. The model involves conceptualizing tissues of various densities as mixtures of 2 appropriate materials.<sup>6,10,16</sup> In order to simplify the extraction of water equivalent length per pixel, the CT number interval is divided into 2 sub-regions. For CT numbers less than 0, the tissue producing the observed CT number is assumed to be a mixture of air and water.<sup>10</sup> Since both of these materials have very nearly the same  $Z$  and  $Z/A$ , the CT number is proportional to the water equivalent pathlength. Fat, which has a  $Z$  of 6.2 is the potential problem in this interval.<sup>13</sup> However, using eqn 1, calculations show that the lower  $Z$  is offset somewhat by a higher  $Z/A$ , resulting in a net error in the calculated water equivalent length for fat of about 1.5%.

For CT numbers greater than zero, the mixture is assumed to have a well defined correlation between density and atomic number. This assumption reduces the number of independent variables to one, thus allowing for the water equivalent range of bone to be extracted from a single energy CT scan. The rationale for this model rests on the assumption that intermediate density bone may be thought of as a mixture of water and compact bone. Furthermore, a realistic bone analogue material is needed for the calibration. Dibasic potassium phosphate is such a material, and is a water soluble bone analogue material<sup>16</sup> with physical density and attenuation properties very similar to the principal mineral in bone, namely calcium hydroxyapatite.

Calibration curves converting CT number to water equivalent path length per pixel appear in Fig. 2.f. These data were obtained by CT scanning the phantom materials and then placing the samples in a

†General Electric 7800 scanner, EMI 5005 scanner

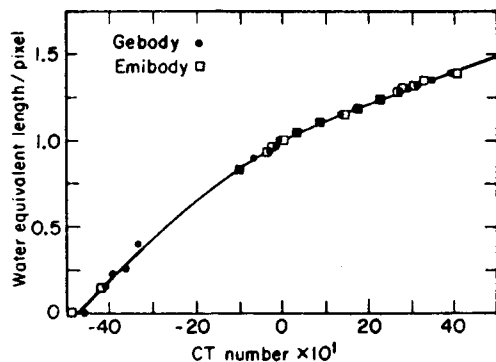


Fig. 2. Calibration curve relating CT number from EMI and GE scanners to water equivalent range per pixel.

helium ion beam to measure the relative water equivalent range. Tissue phantom materials used in the calibration included (1) solutions of water and potassium phosphate to simulate a variety of bone densities, (2) alcohol and water mixtures to simulate adipose tissues, and (3) phantom lung and cork to simulate low density tissues. The GE scanner was operated at 120 KVP and the EMI scanner was run at 140 KVP during both calibration and patient scans. Both curves exhibit 2 general slopes, one associated with CT values less than zero, and a lower slope correlated with the high CT range. The decreased slope for bone may be explained by the  $Z^3$  dependence of the photoelectric effect contributing strongly to CT values, while  $Z$  dependent effects contribute to the water equivalent length only weakly through the log term in eqn 2.

Note that both scanners have a limited dynamic range for high density measurements. A CT number of 500 corresponds to a water equivalent range of 1.5. Furthermore, bone with a higher water equivalent length is interpreted by the scanner as having the same CT number, since this is the maximum value recorded. Fortunately the number of pixels with a CT number equal to 500 is negligibly small. An analysis of scan numbers of a coronal head scan through the base of the skull showed that less than 0.5% of the pixels had CT numbers greater than 490. Although this analysis is subject to errors from finite slice thickness and partial averaging, the result suggests that the amount of truly dense bone (with a density greater than 1.5) is quite small and distributed in thin shells rather than concentrated in a single volume.

The quantitative CT data are sensitive to additional factors, such as sampling position, systematic calibration drift, and artifacts. The calibration data were

taken in a 25 cm diameter cylindrical water phantom with sample vials symmetrically placed within the circumference. In order to test the influence of bone shape on CT values, selected samples were also placed in an anthropomorphically shaped phantom and scanned. When identical bone solutions were placed in different locations of the body phantom 3 per cent differences in CT values were measured. No corrections for these variations are made in conversion of CT data to water equivalent range. Calibration shifts were also detected over a period of about a year. These drifts have been measured to be as large as 3%. To circumvent this source of error calibration scans are taken before patient scans.

Cupping artifacts are found in CT data near bone/tissue interfaces and other high/low density regions. This effect is manifested by an apparent decrease of CT numbers extending several pixels into the bone with a corresponding increase of CT numbers in the region from the interface into the tissue. Range calculations of beams perpendicular to the interface will not be influenced by the artifact since the CT effects on either side of the interface tend to balance each other. Calculational errors produced on tangential rays by this effect have yet to be studied.

The accuracy of the single energy technique in range determination was tested by CT scanning an anthropomorphic phantom,<sup>†</sup> calculating the anterior posterior water equivalent range of the body section using the calibration curve, and comparing these results with experimentally measured ranges using the Bragg peak shift seen in the helium ion beam. The results of this study appear in Fig. 3. In general, agreement between calculation and experiment is within 3%, with a suggestion that a systematic error is present.

This systematic error of 1.5% may be due to the difference in the relative stopping power between water and the phantom material. The phantom is made from isocyanate rubber, which is oxygen deficient. Over 50% of the oxygen content in water or muscle is replaced with carbon in this compound.<sup>15</sup> The largest difference in Fig. 3 between calculated and experimental range appears to be about 5%.

The present level of accuracy is sufficient for most abdominal and pelvic irradiations. A 3% error with a typical residual range of 20 cm yields a 6 mm uncertainty in the stopping point of the beam. This amount is ordinarily included within the margins of the target volume as defined by the radiotherapist. Improvements in the calibration curve and elimination of the systematic difference could improve the stopping point uncertainty by a factor of 2.

<sup>†</sup>Alderson Rando phantom

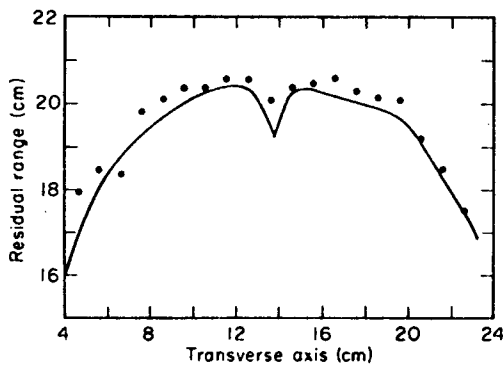


Fig. 3. A comparison of the CT predicted water equivalent range (line) and measured range of a Rando phantom slice of the abdomen (points). The beam was passed through the section from an anterior port.

#### Treatment planning code

A computer program was written to calculate isoeffect or physical dose distributions for heavy ion irradiations. The quantities specified for each port include particle type, direction, field size, residual range, ridge filter, weight, field position and data files describing external compensation. Any number of static ports may be specified. The density matrix of water equivalent path lengths is generated by use of the calibration curve. This array is an  $80 \times 80$  matrix obtained from compressing the original  $320 \times 320$  scan data. The pixel dimensions are a function of the specific scanner, but generally are about 0.5 cm after the matrix compression. The principal beam transport algorithm is based on range shortening by tissues and inhomogeneities. Given the residual range, the water equivalent length of each successive pixel is subtracted to obtain the new residual range. For oblique fields, the partial path through each pixel is calculated. The dose at each pixel is calculated by a look up table relating residual range with central axis dose. An additional quantity calculated in each plan is the per cent integral dose. This is defined as the sum over all pixels of the per cent dose times the water equivalence factor of each pixel. This differs from the quantity of integral dose in that it is calculated only within the particular slice. However, the per cent integral dose per slice is useful in evaluating the advantages of various multiple port configurations in the selection of an optimal field arrangement. The treatment plan giving 100% to the target volume with the lowest per cent integral dose is generally preferred over other plans, assuming critical structures are avoided.

The dose calculation algorithm does not include effects from multiple Coulomb scattering. Heavy charged particles undergo small angle scattering as do all charged particles. However, for heavy ions, the scatter angles and lateral displacements are small

relative to lighter particles such as pions and electrons. Under most conditions, multiple Coulomb scattering does not affect the resulting isodose distributions. Regions where this effect is noticeable include regions near the boundary of tissues with greatly differing densities, such as the mediastinum-lung interface. In this region, scattered particles may traverse drift spaces and affect the dose laterally adjacent to beam rays. Dosimetry studies are needed to quantify these effects.

The dose enhancement and depletion near sharp edges has been studied experimentally with the helium ion beam to determine the magnitude of this effect and the need for its inclusion in dose calculation schemes. Dose perturbations near a 1 inch slab of lucite in air measure about 6% in magnitude. The geometry used for these measurements is described elsewhere.<sup>8</sup> This value is not nearly as large as the theoretically possible  $\pm 50\%$  dose perturbations<sup>5</sup> because of the non-parallel nature of the beam. The small amount of beam divergence which degrades the dose perturbation results from small angle scatter as the beam passes through beam elements such as the ridge filter and water column. Since the edge effect is small for our beams, algorithms for calculating these perturbing effects are not included in the dose calculations.

A mini computer with 96 K words of core memory, floating point processor, a 33 megabyte disk drive and graphics display are the components used for treatment planning. The program is written in Fortran IV, and a typical treatment plan requires 6 min of computation to produce the dose matrix. An additional 5 min are needed to obtain a hard copy of the treatment plan on an electrostatic printer-plotter. In this form, isodose and isoeffect contour lines are superimposed on a grey level image of the CT slice. Calculations are set up in batch mode to facilitate the computation of several planes in the treatment volume without operator intervention.

## RESULTS

#### Representative treatment plans

Treatment plans are included which show representative portals for the irradiation of the outlined target volumes. These plans however, do not show the only possible portal arrangements utilized in clinical irradiation since patient condition and previous treatments may dictate the use of particular fields. Only 1 slice per site is displayed here although in practice, multiple slices are calculated in order to appreciate the dose distribution in 3 dimensions. In these plans, the CT data are assumed to depict the correct relative location of tumor to normal tissues. This is not strictly true in our case since patients presently are scanned in a recumbent position, while

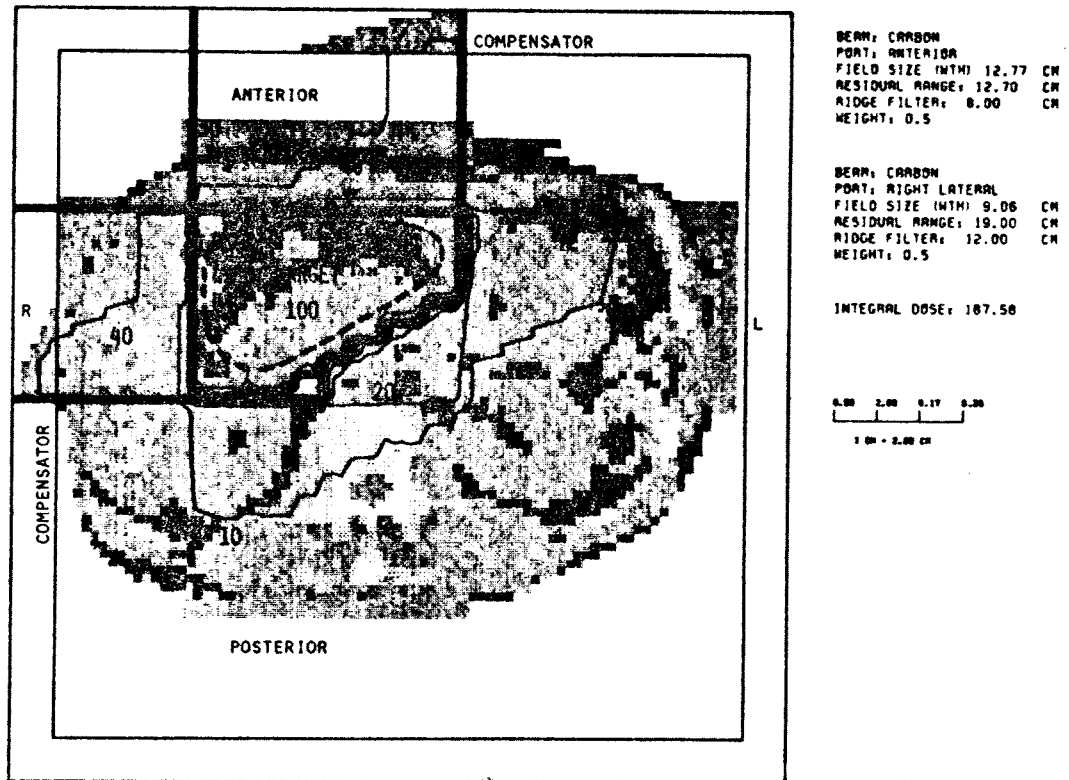


Fig. 4. A treatment plan for the irradiation of the pancreas with a carbon beam.

many of them are treated upright (because of the limitation of a fixed horizontal beam).

With these limitations in mind, treatment plans are now presented for the irradiation of the pancreas, para-aortic nodes, pelvis, and esophagus. Each plan contains isoeffect contours ranging from 10 to 100% in 10% increments of Core dose. The irradiation parameters for each port are also given, including ion type, beam direction, weight, and field width, residual range in cm of water, and ridge filter in cm. The per cent integral dose of the plan for each slice is also calculated.

#### *Pancreas*

Figure 4 shows a treatment plan for the irradiation of a pancreatic lesion with carbon ions. Equally weighted anterior and lateral ports are used for this particular tumor location. In addition to a surface flattening bolus, a simple wedge shaped compensator is used in both ports to shape the high dose region around the distal contour of the target volume. The artificial step like dose gradient posterior and distal to the target results from the finite pixel size used to describe the compensation. In practice, the compensator would be constructed as a smooth wedge, not as a step wedge.

In the abdomen, the major types of tissues and inhomogeneities encountered are soft tissue, fat, rib and bowel gas. From an analysis of pixels in the beam path, the areas traversed by the charged particle

beams have an average density of 1.0 g/cc. Varying amounts of fat along rays will produce range variations of approx. 0.5 cm. Although ribs are present in the lateral portal, they perturb the beam minimally, on the order of 3 mm. This is consistent with an expected 1 cm path length through a given rib, which typically would have a density of 1.3 g/cc. in its density areas.

The target volume in this plan is irradiated uniformly to 100% while tissues proximal to the target are dosed to 40%. The spinal cord, one kidney and portions of the gut receive up to a 10% exit dose from the beam fragmentation tail. These critical structures received significantly less dose with charged particles compared with photon irradiation using standard treatment plans. A 3 field variation of this plan was also calculated, but appeared to produce no advantage over the 2 field for the target shown. Although the proximal areas were given about 10% less dose in the 3 field plan, a large region of intestinal tract was necessarily irradiated to about 30%. In addition, the per cent integral dose for the 3 field plan was 8% higher. If the lesion were more centered with respect to midline, a 3 field plan would be acceptable.

#### *Esophagus*

The primary inhomogeneities involved in the irradiation of an esophageal lesion are the lungs, trachea, bronchi, sternum and ribs. As Fig. 5 shows, the thorax presents a number of regions with vastly

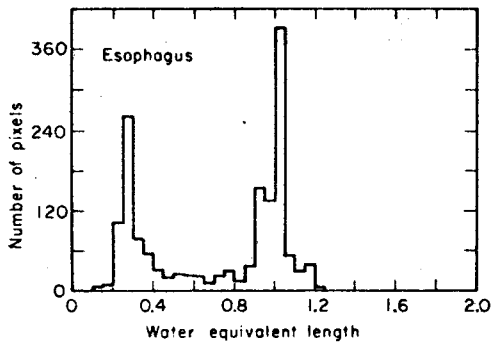


Fig. 5. Histogram of the water equivalent ranges of pixels within the irradiated volume of an esophageal lesion.

different densities. This histogram of pixels within the beam paths reveals a soft tissue peak at 1.02 g/cc. with a large peak resulting from lung at 0.27 g/cc. The pixels with intermediate densities between 0.5 and 0.77 g/cc. are located at the edges of the lung and at the anterior body surface. These densities result from both partial sampling and respiratory motion during the CT scan.

A neon ion treatment plan for the esophagus is shown in Fig. 6. Three equally weighted and compensated fields are used in this conedown irradiation. The anterior and right portals have wedge shaped compensators which pull the dose gradient away from

the spinal cord. Again, the target volume is uniformly treated to 100% with an average mediastinal dose of 25% and average lung dose of 35%. The spinal cord receives 10% from the fragmentation tail of the neon beam.

Aside from the wedge compensators, only a flattening bolus is used to produce isodose shaping. Although the path length through lung may vary significantly the resulting isodose distribution from 3 ports is quite suitable for this target volume. Note the irregular isoeffect contour in the lungs resulting from inhomogeneities.

This particular site is amenable to *in vivo* dosimetry. Typically, a multidiode probe housed in a naso-gastric tube is passed down the esophagus to the region of interest, and the charged particle beam is swept through the body (by sweeping the water column) until the distal edge of the beam is detected. Such measurements give information on the required residual range, and furnish experimental verification of calculated residual ranges. These techniques were reported by us elsewhere.<sup>5</sup>

#### Para-aortic nodes

Para-aortic nodes are technically difficult to irradiate with photons because in most techniques either the spinal cord or kidneys reach tolerance dose

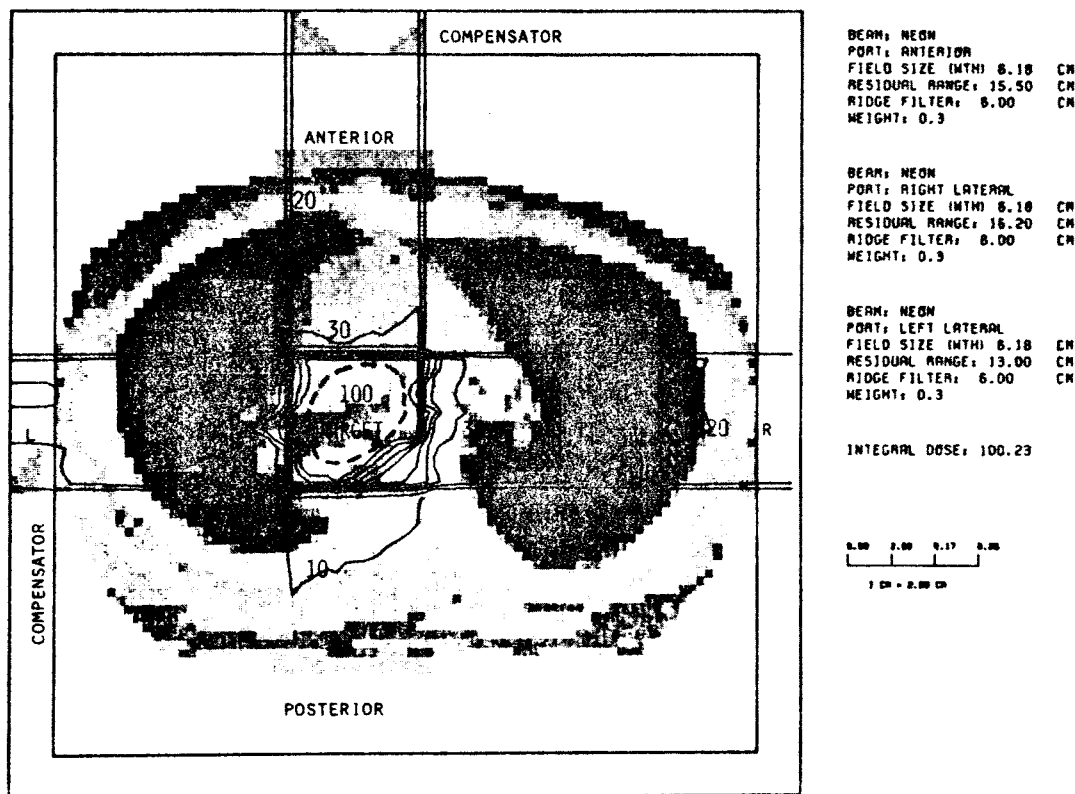


Fig. 6. A 3 field treatment plan for an esophageal lesion using a neon beam.

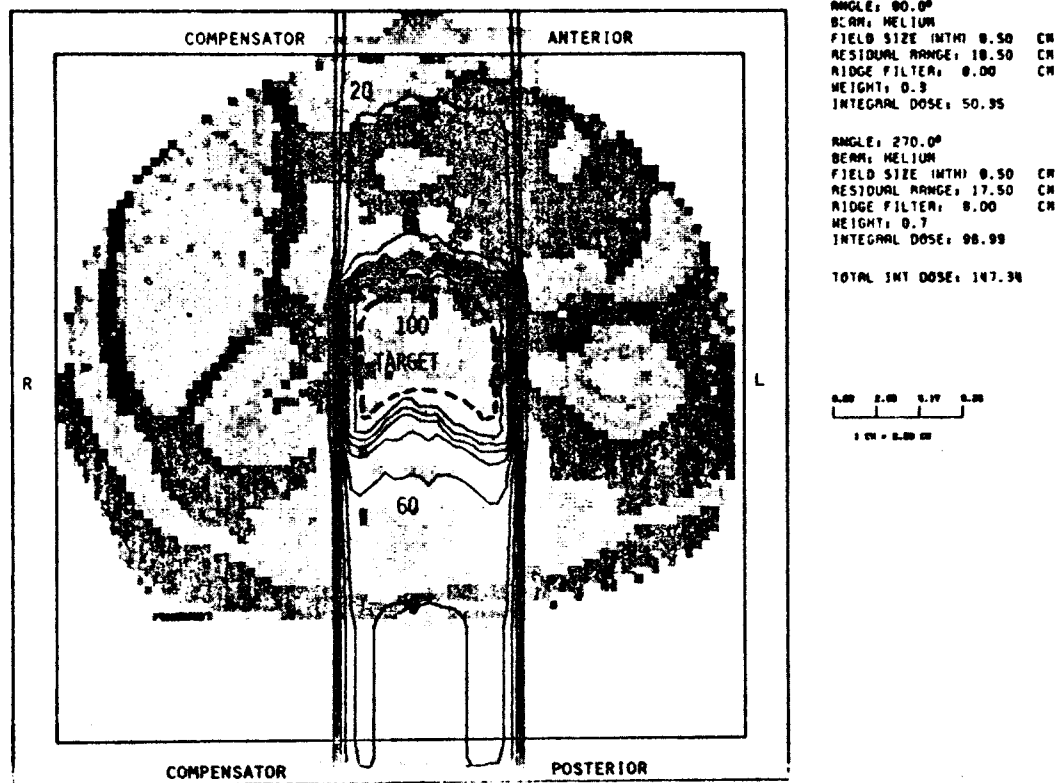


Fig. 7. A treatment plan for the para-aortic nodes. The posterior field is weighted 2:1 relative to the anterior field.

before an adequate dose is given to the nodes. These limiting factors may be reduced by the use of heavy ion beams. A proposed scheme for the irradiation of the para-aortic nodes with helium ions is presented in Fig. 7. A pair of parallel opposed fields are used, weighted 2:1 in favor of the posterior field. The target volume is uniformly irradiated to 100% with this field configuration while the anterior intestinal tract receives 30% and the spinal cord receives about 60%. In this plan, compensation was used to shape the high dose region around the irregularly shaped target. The use of a cord compensator in the anterior field pulls the steep dose gradient away from the spinal cord and cauda equina while the tumor is still covered adequately.

The use of a direct posterior field necessarily includes irradiation through the vertebral body. This bony inhomogeneity may pull back the beam by as much as 1.5 cm. The calculated range shortening by a vertebral body is shown in Fig. 8. The image of this bony inhomogeneity is represented in hexadecimal form, where each character represents a particular water equivalent range. The pixel size in this image is 1 mm × 1 mm. The level of the display has been elevated to show only the vertebral body. With the posterior entrance surface bolussed flat, the residual range was set to give sufficient penetration to totally traverse the inhomogeneity. The asterisks at the top

of the figure represent the calculated stopping point of the beam. A comparison of those rays which passed through the vertebral body with those which passed only through soft tissue shows a maximum range shortening here of 1.0 cm. The calculated range shortening for a number of vertebral bodies has been compared with experimental measurements using film stack techniques,<sup>5</sup> and both experiment and calculation agree within expected uncertainties. The observed range shortening spans the interval 1.0-1.6 cm.

#### Pelvis

Figure 9 shows a treatment plan for the irradiation of a large pelvic lesion with carbon. In this site the beams must penetrate through the iliac crest before reaching the target. A pixel by pixel analysis of the CT scan shows that within the beam paths, approximately 25% of the pixels are fat, and about 17% of the pixels are bone with an average density of 1.17 g/cc. Data in the form of a histogram appear in Fig. 10.

A 3 field portal arrangement has been chosen for this irradiation. The carbon beam is perturbed most in the posterior port, which must traverse the high density bone in the posterior region of the left iliac crest. From this direction, the range shortening may be as great as 2 cm as compared with soft tissue paths. Compensation has been added to shape the high dose

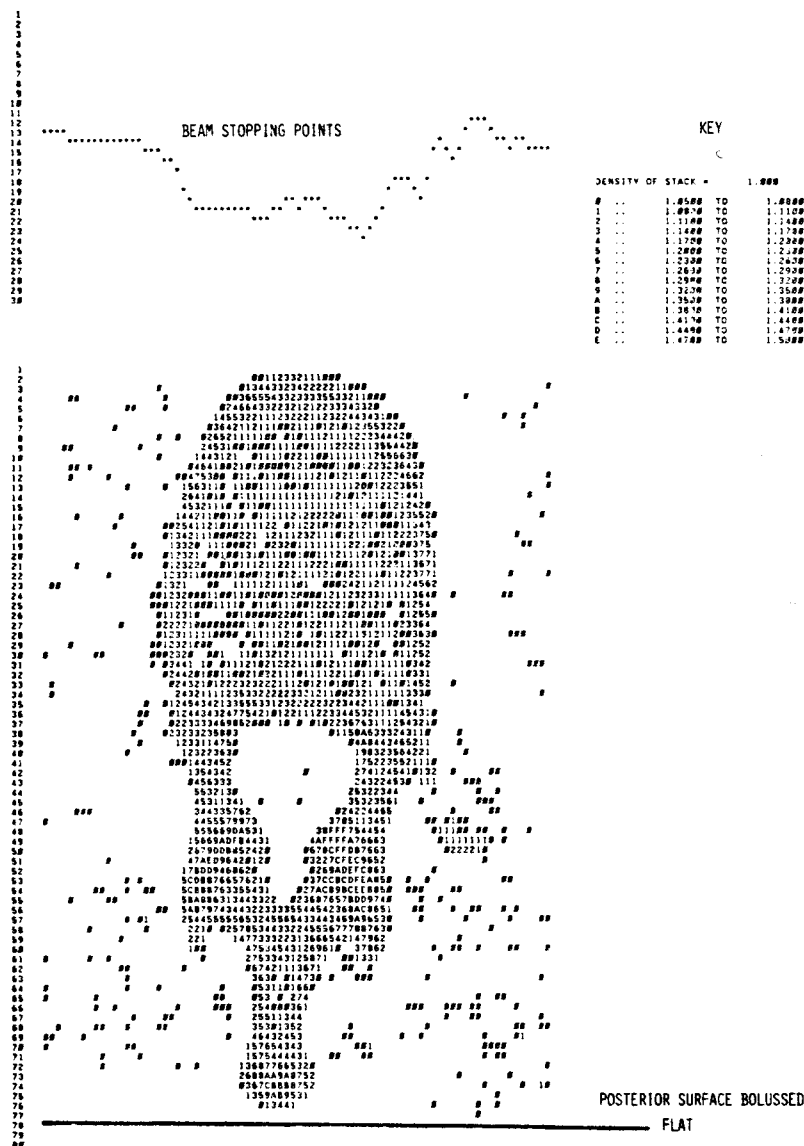


Fig. 8. The calculated range shortening by a vertebral body.

region to a circularly shaped tumor. The use of heavy ions here has reduced the dose to the bladder and part of the intestinal tract.

**DISCUSSION**

This effort represents the first version of a charged particle treatment planning program. Several areas of the program will be improved in the near future. The treatment planning process will be modified to allow for interactive use through target volume delineation with a cursor and CT graphics display hardware. This will enable the therapist to enter the desired target volume on several sequential CT slices. Such information will be used to shape the appropriate portal collimators and the contour information will be used to design three dimensional compensation. Increase in calculational speed will permit the therapist and physicist to rapidly calculate a selection of portal arrangements and display

intermediate isodose distributions on the graphics unit before final selection of the optimal plan.

Other areas for program improvement include the incorporation of respiration effects on dose distributions, and the possible misalignment of compensation. Computer simulation of beam scanning systems is also planned. The present technology of dose delivery requires the selection of a ridge filter whose width is determined by the maximum depth of the tumor along the beam axis. This constrains us to use a ridge filter which has an inappropriate width in other planes of interest. One solution to this constraint is to eliminate the use of fixed ridge filters and use a raster scanning pencil beam with variable ridge filter. At each raster point, the depth of penetration and dose, as well as the ridge filter width would be altered dynamically to produce the resulting desired dose distribution. With computer simulation of this

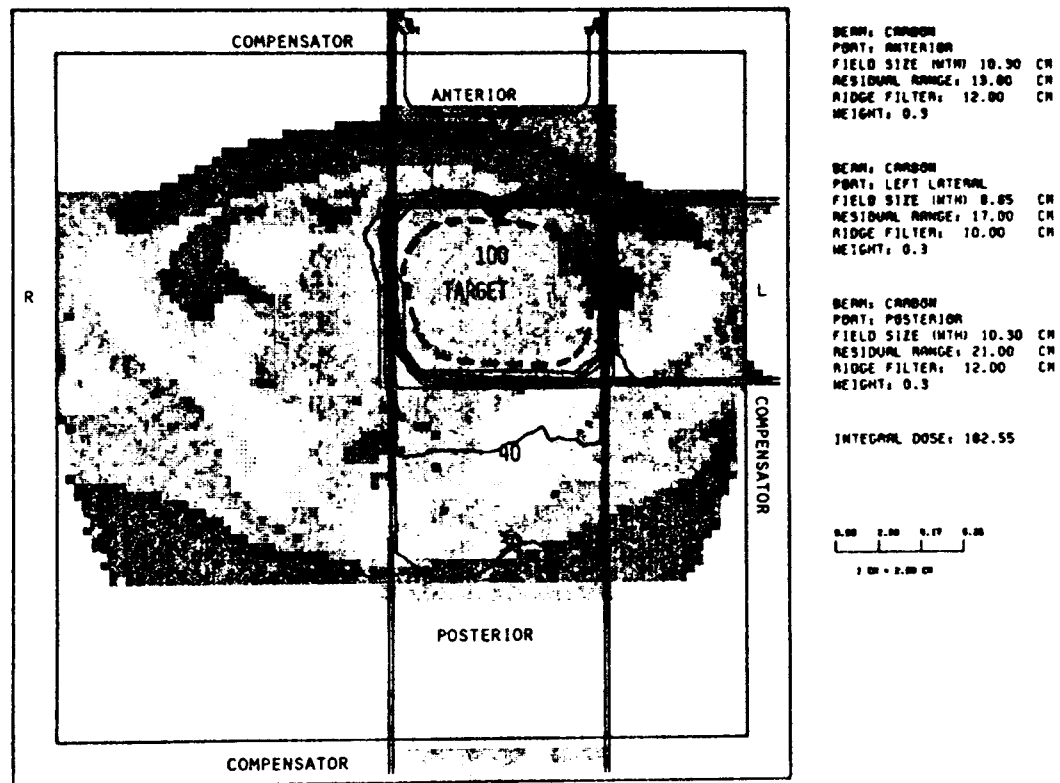


Fig. 9. Treatment plan for a pelvic mass with carbon beams.

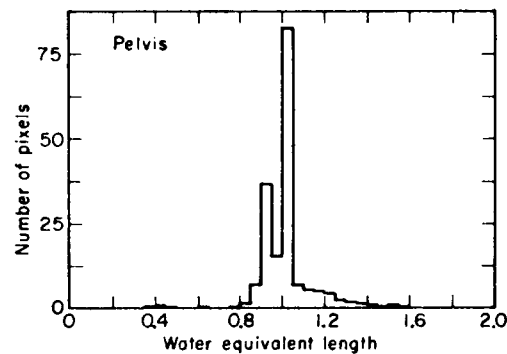


Fig. 10. Histogram of water equivalent ranges of each pixel within the irradiated volume in the pelvis case.

system, it will be possible to explore the advantages of beam scanning over fixed ridge filter systems, and

to define the performance specifications suitable for charged particle therapy.

#### REFERENCES

1. Bischel, H: Passage of charged particles through matter, *Am. Instit. Phys. Handbook*, McGraw-Hill, 1972, Sect. 8, p. 142.
2. Blakely, E.A., Tobias, C.A., Yang, T.C., Smith, K.A.: Cell survival parameters for extended Bragg peaks. *Rad. Res.* (abstract) 74: 588, 1978.
3. Castro, J.R., Quivey, J.M.: Clinical experience and expectations with helium and heavy ion irradiation, *Int. J. Oncol. Biol. Phys.* 3: 127-131, 1977.
4. Castro, J.R., Quivey, J.M., Lyman, J.T., Chen, G.T.Y., Kanstein, L., Walton, R.: Heavy Ion Radiotherapy, Report No. 5610, Berkeley, California, Lawrence Berkeley Laboratory, 1977, pp. 198-218.
5. Chen, G.T.Y., Lyman, J.T., Quivey, J.M., Castro, J.R.: Analysis of dose perturbations by vertebral bodies in charged particle radiotherapy. *Med. Phys.* 4: (abstr.) 334, 1977.
6. Genant, H.K., Boyd, D.: Quantitative bone mineral

- analysis using dual energy computerized tomographic scanning. *Invest. Radio.* 12: (abstract) 545, 1977.
7. Goitein, M.: A technique for calculating the influence of thin inhomogeneities on charged particle beams. *Med. Phys.* 5(4): 258-264, 1978.
  8. Goitein, M., Chen, G.T.Y., Ting, J.Y., Schneider, R.J., Sisterson, J.M.: Measurements and calculations of the influence of thin inhomogeneities on charged particle beams. *Med. Phys.* 5(4): 265-273, 1978.
  9. Hubbell, J.H.: Photon cross sections, attenuation coefficients and energy absorption coefficients from 10 to 100 KeV, Natl Standards Reference Data System Natl Bureau of Standards 29, Washington D.C., U.S. Govt. Ptg Office, 1969, p. 70
  10. Kijewski, P.K., Bjarngard, B.E.: The use of computed tomography data for radiotherapy dose calculations. *Int. J. Radiat. Oncol. Biol. Phys.* 4: 429-435, 1978.
  11. Raju, M.R., Gnanapurani, M., Martins, B., Howard, J. Lyman, J.T.: Measurement of OER and RBE of the 910 MeV helium ion beam using cultured cells. (T1). *Radiology* 102: 425-478, 1972.
  12. Rutherford, R.A., Pullan, B.R., Isherwood, I.: Measurement of effective atomic number and electron density using an EMI scanner. *Neurorad* 11: 15-21, 1976.
  13. Spiers, J.: Effective atomic number of tissues and phantom materials. *Br. J. Radiol.* 19: 52-63, 1945.
  14. Weber, J., van den Berge, D.J.: The effective atomic number and the calculation of the composition of phantom materials. *Br. J. Rad.* 42: 378-383, 1969.
  15. White, D.R.: Tissue substitutes in experimental radiation physics. *Med. Phys.* 5: 467-479, 1978.
  16. Witt, R.M.: Bone standards for the intercomparison of photon absorptiometric bone mineral measuring systems. *Proc. Int. Conf. on Bone Mineral Meas.* (Chicago, 1973), DHEW Pub. No. 75-883, Published by U.S. Dept. HEW, Washington, D.C. p. 114-122.